NANO LETTERS

Letter

pubs.acs.org/NanoLett

Nontoxic and Abundant Copper Zinc Tin Sulfide Nanocrystals for Potential High-Temperature Thermoelectric Energy Harvesting

Haoran Yang,[†] Luis A. Jauregui,[‡,§] Genqiang Zhang,[†] Yong P. Chen,[‡,§,∥] and Yue Wu*[,†]

[†]School of Chemical Engineering, [‡]School of Electrical and Computer Engineering, [§]Birck Nanotechnology Center, and [∥]Department of Physics, Purdue University, West Lafayette, Indiana 47907, United States

ABSTRACT: Improving energy/fuel efficiency by converting waste heat into electricity using thermoelectric materials is of great interest due to its simplicity and reliability. However, many thermoelectric materials are composed of either toxic or scarce elements. Here, we report the experimental realization of using nontoxic and abundant copper zinc tin sulfide (CZTS) nanocrystals for potential thermoelectric applications. The CZTS nanocrystals can be synthesized in large quantities from solution phase reaction and compressed into robust bulk pellets through spark plasma sintering and hot press while still maintaining nanoscale grain size inside. Electrical and thermal measurements have been performed from 300 to 700 K to understand the electron and phonon transports. Extra copper doping during the nanocrystal synthesis introduces a significant improvement in the performance.

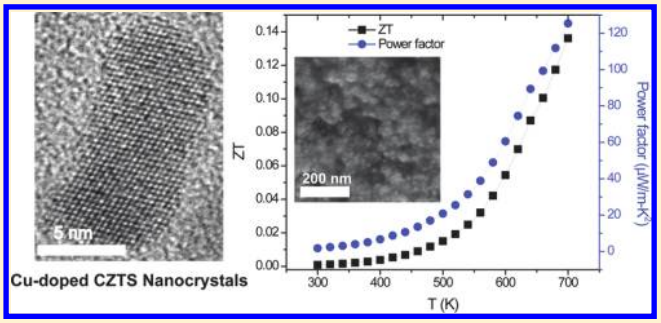

KEYWORDS: *Thermoelectric, copper zinc tin sulfide, nanocrystal, nontoxic, abundant, doping*

The past decade has witnessed the rapid progress of developing various thermoelectric (TE) materials for waste heat recovery and solid-state cooling. However, most of these TE materials are the tellurides or antimonides of transition metals or contain rare earth elements.[1] The limited natural reserve, high raw material cost, and toxicity associated with these compositions could set a barrier for large-scale deployment of TE devices to improve the energy efficiency in various areas ranging from the automobile industry to household heating and cooling. The performance of thermoelectric materials can be rated through a dimensionless quantity called figure of merit or ZT ($ZT = \sigma S^2 T/\kappa$, where σ, κ, S, and T stand for electrical conductivity, thermal conductivity, Seebeck coefficient, and absolute temperature, respectively. T is the average temperature between the hot and the cold sides. Up to now, the best-commercialized thermoelectric bulk material (Bi_2Te_3-based alloy) has a ZT around 1,[2,3] whereas a ZT around 4 is required for a TE device to be competitive with traditional combustion engines or compressor-based refrigeration.[4] In nanostructured materials, the thermal conductivity (κ) could be dramatically reduced through phonon scattering at grain boundaries,[2,3] while the power factor ($P = \sigma S^2$) could be significantly enhanced through quantum confinement or energy filtering.[5] Enhanced ZT above 1 has been observed experimentally in nanostructures including two-dimensional (2D) superlattics,[6−10] quantum dots embedded in matrices,[11−16] and sintered nanocomposites,[17−19] however most of these systems require a complicated and expensive fabrication process, which also limits the possibility of the wide application of thermoelectric devices. So, one of the most challenging aspects in this area is to find a thermoelectric material made from earth abundant elements and with environmentally benign composition, which can be made in a nanostructured form in large quantities and be processed into a robust bulk structure through facile and cost-effective methods. In this report, we have explored the potential of using the nanostructures of copper zinc tin sulfide (CZTS) as a nontoxic and abundant thermoelectric material and characterized its thermoelectric properties between 300 and 700 K. Compared to the traditional telluride- and antimonide-based thermoelectric materials, the elements in the composition of CZTS are in extremely high abundance—the natural reserves of copper, zinc, tin are 630, 250, and 5.2 million tons, while the natural reserves for tellurium and antimony are only 0.022 and 1.8 million tons, respectively.[20] In addition, the threshold limit values (TLV, meaning that the level of a chemical substance to which a worker can be exposed day after day for a working lifetime without adverse health effects) of copper, zinc, and tin are 1, 0.8, and 2 mg/m^3, which are much higher than tellurium and antimony (0.1 and 0.5 mg/m^3, respectively), presenting significant advantages in low toxicity.[21]

Our synthesis of colloidal CZTS nanocrystals involves a one-pot solution phase reaction using copper acetylacetonate, zinc acetate dihydrate, tin chloride, and sulfur as precursors in a solution of oleylamine, which is modified from a previous report.[22] In a typical synthesis, 0.52 g of copper acetylacetonate (97%), 0.20 g of zinc acetate dihydrate (reagent grade), 0.19 g of tin chloride (98%), and 0.13 g of sulfur (99.5%) are added to 40 mL of oleylamine in a 50 mL three-neck flask on a Schlenk

Received: May 20, 2011
Revised: December 15, 2011
Published: January 3, 2012

   dx.doi.org/10.1021/nl201718z | *Nano Lett.* 2012, 12, 540−545

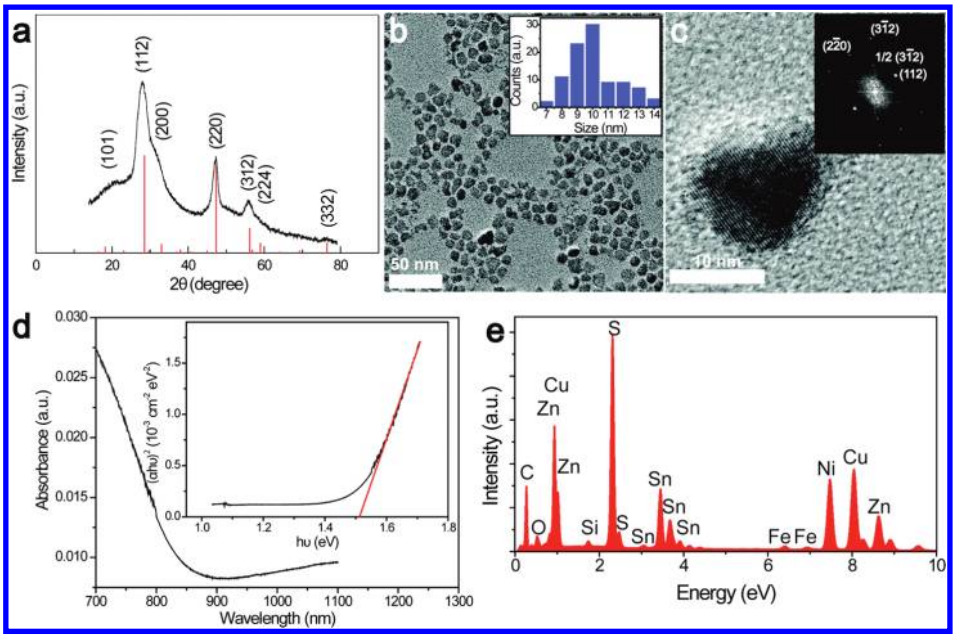

Figure 1. Characterization of CZTS nanocrystals. (a) XRD diffraction pattern of CZTS nanocrystals, which can be indexed into tetragonal CZTS (JCPDS 26-0575, red lines). (b) TEM image of CZTS nanocrystals with an average diameter of 10.6 ± 1.9 nm. Upper inset shows size distribution of CZTS nanocrystals. (c) HRTEM image of a typical CZTS nanocrystal. Inset is 2DFT of the image showing the [44$\bar{1}$] zone axis of CZTS. The 1/2 {312} reflections, although forbidden in bulk CZTS, arise as a result of the finite size of the nanocrystals. (d) UV−vis absorption spectrum of CZTS nanocrystals. Inset, The plot of $(\alpha h\nu)^2$ versus $h\nu$ shows a direct band gap of 1.51 eV. (e) EDX spectrum of CZTS. Ni signal comes from the TEM grid and Fe signal comes from TEM instrument. Notably, the extra Fe peaks are detected because our TEM is using the latest ultrasensitive silicon drift EDX detector with 80 mm collection window. Control test from a blank TEM gird also shows the Fe signal (data not shown).

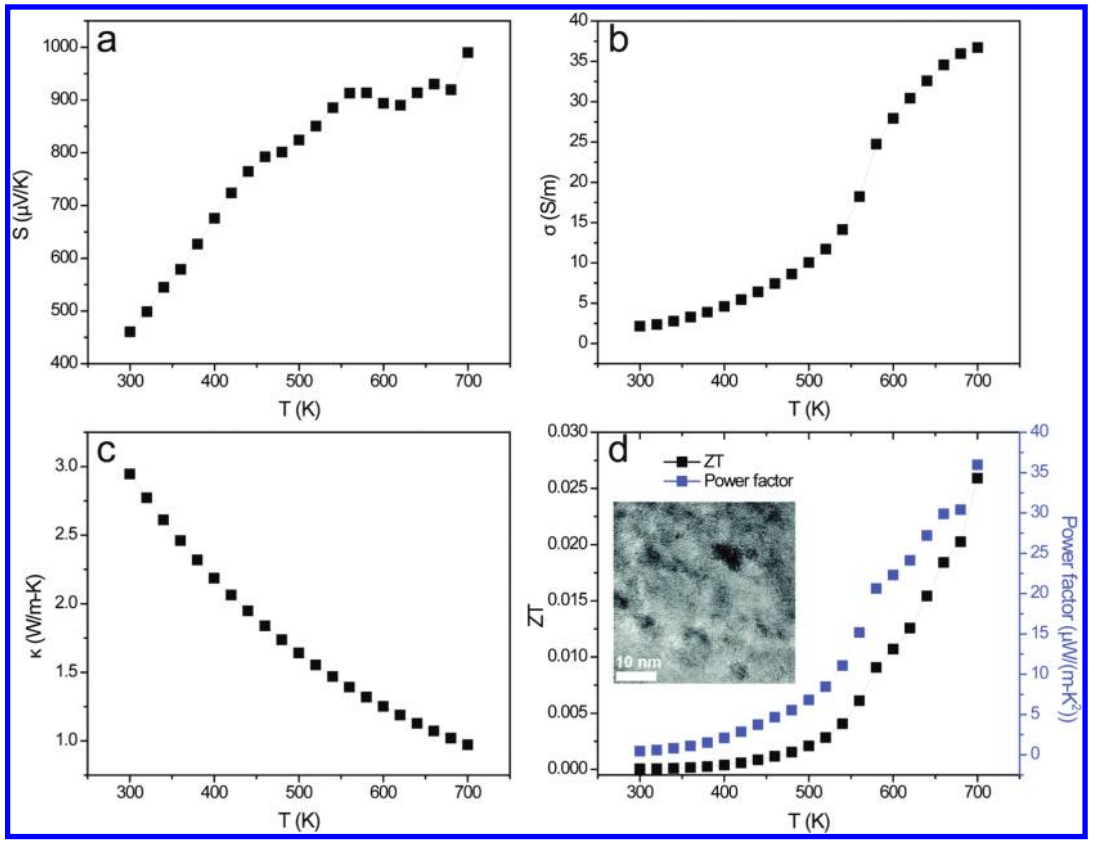

Figure 2. Temperature dependence of thermoelectric properties of undoped CZTS nanocrystal disks fabricated by SPS including (a) electrical conductivity, (b) Seebeck coefficient, (c) thermal conductivity, and (d) power factor and ZT from 300 to 700 K. Inset of (d) shows the HRTEM image on the SPS sintered CZTS with nanocrystalline domains.

dx.doi.org/10.1021/nl201718z | *Nano Lett.* 2012, 12, 540−545

line. The reaction mixture is degassed under vacuum for 2 h, purged with nitrogen for 30 min at 110 °C, heated to 280 °C for 1 h, and then cooled to room temperature. The nanocrystals are precipitated by adding ethanol and followed by centrifugation. In order to remove aggregates of poorly capped nanocrystals, the nanocrystals are redispersed in chloroform and centrifuged again at 8000 rpm for 2 min, and then the precipitation is discarded.

X-ray diffraction (XRD) studies (Figure 1a) show the materials prepared in this way are kesterite phase CZTS (JCPDS 26-0575, Figure 1a, red lines). Low-magnification transmission electron microscopy (TEM) studies (Figure 1b) show uniform nanocrystals with an average size of 10.6 ± 1.9 nm (insert, Figure 1b). High-resolution TEM studies (HRTEM, Figure 1c) confirm that the observed nanocrystals are CZTS and show two important features. First, the TEM data demonstrate clearly that the CZTS nanocrystals are single crystal structures. Second, the reciprocal lattice peaks, which were obtained from 2D Fourier transforms (2DFT) of the lattice-resolved image (insert, Figure 1c) can be indexed to the kesterite phase of CZTS with the zone axes along the $[44\bar{1}]$ direction. Notably, the 1/2 {312} reflections, although forbidden in bulk CZTS, arise as a result of the finite size of the nanocrystal.[23,24]

The optical properties of the CZTS nanocrystals have been studied by UV−vis absorption spectroscopy (Figure 1d). The plot of $(\alpha h\nu)^2$, the square of the absorption coefficient (α) multiplied by the photon energy ($h\nu$) versus $h\nu$ (inset, Figure 1d), shows a direct band gap of 1.51 eV which is larger than the reported bulk value (1.40−1.49 eV),[25,26] suggesting the presence of a quantum confinement in band structure due to size or strain effect.[27] Notably, such an increase in band gap is also consistent with the previous reports on CZTS nanocrystals as well.[28,29] In addition, energy dispersive X-ray spectroscopy (EDX, Figure 1e) has also been used to further characterize the composition of the nanocrystals, which gives a formula of $Cu_2Zn_{0.98}Sn_{1.21}S_{4.36}$. The extra sulfur in the EDX result could come from the enhancement effect where the secondary X-rays emitted by heavier elements are sufficiently energetic to stimulate additional secondary emission from lighter elements.[30]

We have explored the potential thermoelectric application of CZTS nanocrystals by fabricating devices through spark plasma sintering (SPS) of CZTS nanocrystal powder into solid disks with 1 in. diameter and 0.1 in. thickness. In a typical fabrication process, we first remove the capping ligands on the nanocrystal surface by mixing the CZTS nanocrystals dispersed in toluene and diluted hydrazine/acetonitrile solution (1% volume ratio) with vigorous stirring until the nanocrystals were totally precipitated. The supernatant is decanted, and the precipitant is washed with ethanol three times to remove the hydrazine and acetonitrile. After the hydrazine treatment, the nanocrystals are collected by centrifugation, dried in vacuum, and ground into a powder. CZTS nanocrystal powder is consolidated by SPS at 678 K for 5 min under an axial pressure of 50 MPa and a dc current of 15 kA. Electrical conductivity, Seebeck coefficient, and thermal conductivity of the CZTS nanocrystal-based thermoelectric devices have been investigated between 300 and 700 K. The electrical conductivity (Figure 2a) of the CZTS nanocrystals increases from 2.1 S/m at 300 K to 36.7 S/m at 700 K. Figure 2b shows the temperature dependence of Seebeck coefficient of the CZTS nanocrystals. The positive Seebeck coefficient value indicates the p-type conduction. The Seebeck coefficient measurement shows an increasing trend from 460 μV/K at room temperature to 990 μV/K at 700 K. The thermal conductivity of CZTS nanocrystals is measured through thermal diffusivity and specific heat and then calculated via the equation $\kappa = \alpha\rho C_p$ (α is thermal diffusivity, ρ is the density, C_p is the specific heat). The thermal conductivity (Figure 2c) at 300 K is measured to be 2.95 W/m·K, and it decreases rapidly with the increasing temperature to 0.97 W/m·K at 700 K, which indicates that phonon conductivity is predominant. The calculated ZT for the CZTS nanocrystal (Figure 2d) increases from 4.6×10^{-5} at 300 K to ~0.026 at 700 K.

Analysis of these results highlights some important points. First, the electrical conductivity of our CZTS nanocrystal-based thermoelectric device is lower than the value of the stoichiometric CZTS bulk crystal (529 S/m, without Cu dopping),[25] which may be due to the fact that our CZTS thermoelectric devices are fabricated by SPS at a relatively lower temperature (678 K), while the bulk crystals were usually grown at 1123 K.[25] The high-temperature process will typically promote the growth of the grain and result in larger crystalline domains, which will usually have a higher electrical conductivity. However, we decide to keep our SPS process at low temperature to avoid the uncontrollable copper diffusion at high temperature. Indeed, our TEM studies (inset, Figure 2d) performed on our CZTS samples after the SPS process show that the nanocrystals remain their original size although they have been pressed into bulk pellets. Second, our CZTS nanocrystal devices show a significantly enhanced Seebeck coefficient than the stoichiometric CZTS bulk crystal, which only has a maximum value of 355 μV/K in the same temperature range.[25] Conceptually, the significant enhancement of Seebeck coefficient could be explained by quantum confinement and energy filtering. Quantum confinement gives rise to δ-function-like density of state (DOS) in 0D quantum dots, which differs from the DOS in bulk semiconductors with a wide energy distribution, and it has been predicted that the δ-function-like DOS will lead to a great enhancement of power factor.[31,32] Another possible explanation is through energy filtering, which occurs at grain−grain interfaces where charge carriers encounter a potential barrier, and only those of them with high enough energy could pass the barrier, which also leads to an increased power factor by theoretical prediction.[33] Indeed, our UV−vis measurement (Figure 1d) indicates that our CZTS nanocrystals have a bigger band gap of 1.51 eV compared to the reported bulk value (1.40−1.49 eV), which suggests that a contribution from the quantum confinement may exist. In addition, we have observed the existing of vast grain boundaries in our samples even after the SPS process (inset, Figure 2d), which also indicated that the energy filtering might play a more important role to lead the enhancement in the Seebeck coefficient. Third, the thermal conductivity of our nanostructured CZTS (2.95 W/m·K at 300 K and 0.97 W/m·K at 700 K) is greatly reduced compared to the value from stoichiometric CZTS bulk crystals (4.7 W/m·K at 300 K and 1.21 W/m·K at 700 K),[25] which can be attributed to the increased phonon scattering at nanocrystal grain boundary. Fourth, although the ZT value of the undoped CZTS nanocrystals (ZT~0.026) is still low and similar to the stoichiometric CZTS bulk sample (ZT~0.039), it shows a great potential to be further improved through the copper doping to increase the electrical conductivity. Notably, people have found that the electrical conductivity of CZTS bulk

dx.doi.org/10.1021/nl201718z | Nano Lett. 2012, 12, 540−545

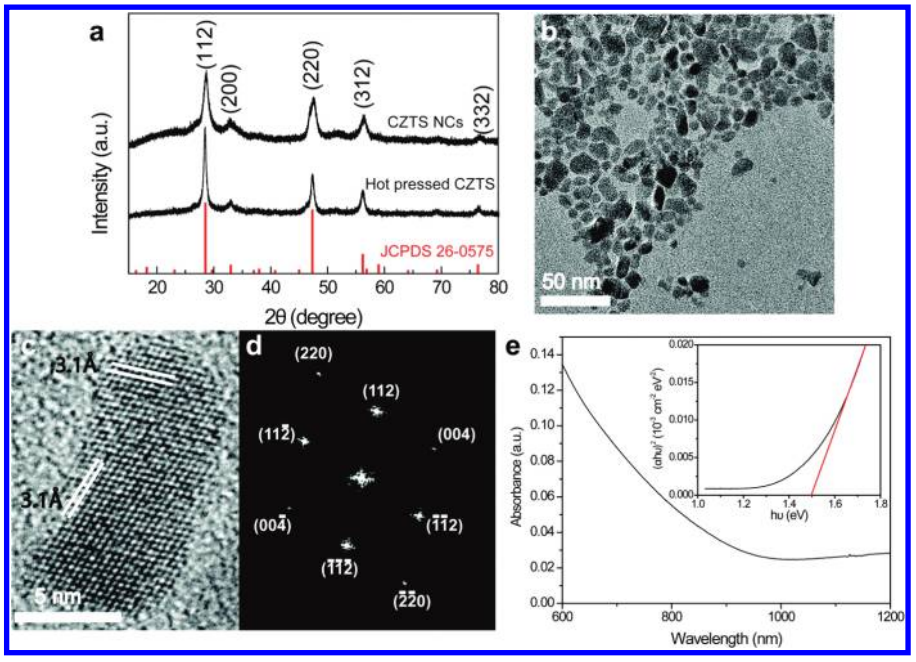

Figure 3. Characterization of Cu-doped CZTS nanocrystals with a composition of $Cu_{2.19}Zn_{0.80}Sn_{0.75}S_{3.53}$. (a) XRD patterns of Cu-doped CZTS nanocrystals (upper) and hot-pressed disk made from them (lower). The red lines correspond to the tetragonal CZTS (JCPDS 26-0575). (b) and (c) TEM images of Cu-doped CZTS nanocrystals. (d) 2DFT of the image shown in (c) reveal the $[1\bar{1}0]$ zone axis of CZTS. (e) UV−vis absorption spectrum of Cu-doped CZTS nanocrystals. Inset shows the plot of $(\alpha h\nu)^2$ versus $h\nu$ has a direct band gap of 1.50 eV, which is smaller compared to the undoped CZTS nanocrystals due to the extra Cu as p-type dopants.

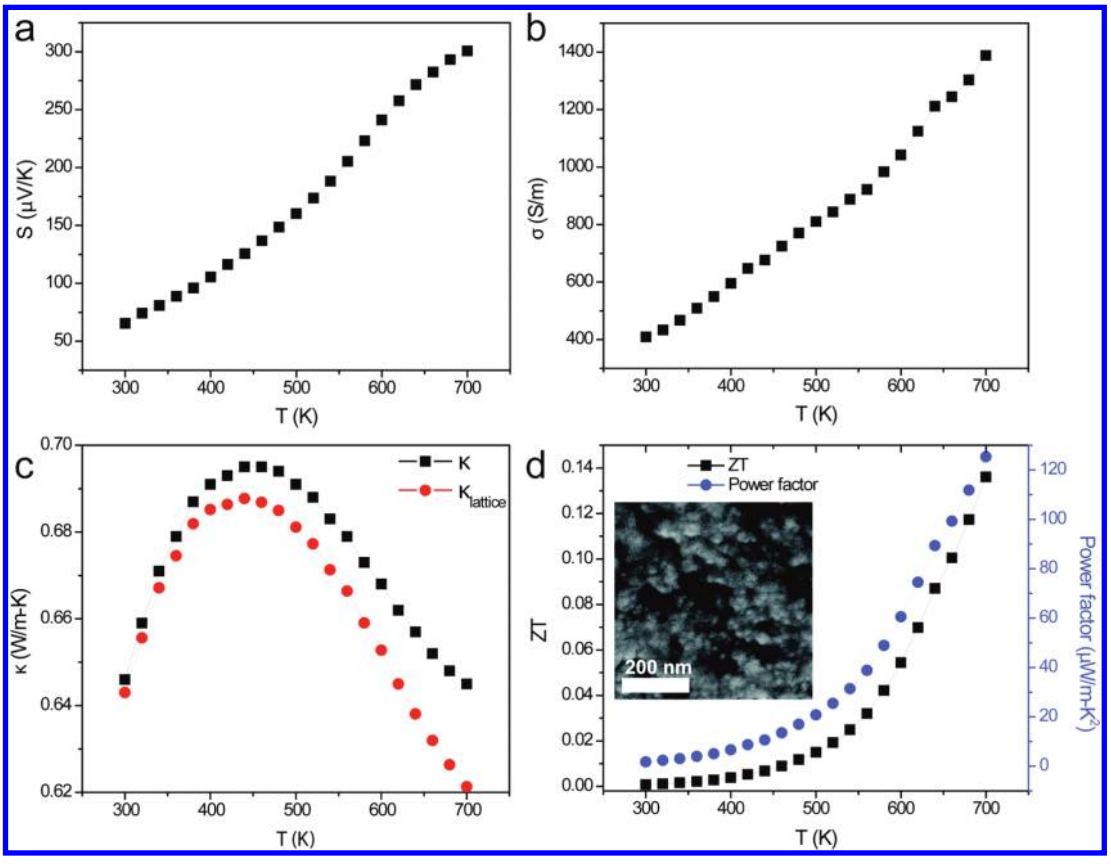

Figure 4. Temperature dependence of thermoelectric properties of Cu-doped CZTS nanocrystal disks fabricated by hot press from 300 to 700 K: (a) Seebeck coefficient, (b) electrical conductivity, and (c) thermal conductivity. The black line is the overall thermal conductivity including both the contribution from electrons and lattice, and the red line is the lattice thermal conductivity. (d) Power factor and ZT. Inset of (d) shows the scanning electron microscopy image on the hot pressed Cu-doped CZTS nanocrystal disk samples with nanocrystalline domains.

dx.doi.org/10.1021/nl201718z | Nano Lett. 2012, 12, 540−545

crystals can be significantly enhanced by almost 25 times through copper doping (up to 5%),[25] which suggests that a higher ZT value could be achievable in our CZTS nanocrystals as well.

In order to investigate the impact of extra copper doping on the electrical and thermal properties of our CZTS nanocrystals, we modify the synthesis recipe by adjusting the relative concentration of initial precusor. More importantly, through mutilple attempts, we found that only by changing the reaction from one-pot synthesis to hot injection can we avoid the "self-purification" effect in the CZTS nanocrystals and stabilize the extra copper dopants.[34,35] In a typical growth, 0.98 g of copper acetylacetonate (97%), 0.295 g of zinc acetate dihydrate (reagent grade), and 0.355 g of tin chloride (98%) are added to 55 mL of oleylamine (OLA) in a 100 mL three-neck flask on a Schlenk line. The mixture is degassed under vacuum at 80 °C for 1 h and purged with nitrogen for 30 min at 110 °C. Meanwhile, 0.195 g of sulfur (99.5%) is dissolved in 5 mL of oleylamine in a separate vial at 100 °C. The solution in three-neck flask is heated to 300 °C when the sulfur in oleylamine solution is injected. After injection the temperature is held for 1 h, and then the reaction mixture is cooled down naturally. The nanocrystals are collected and cleaned in a similar way like the updoped CZTS nanocrystals. XRD studies (Figure 3a) show the materials prepared in this way are still kesterite phase CZTS (JCPDS 26-0575, Figure 3a, red lines). Low-magnification TEM studies (Figure 3b) show that the Cu-doped CZTS nanocrystals have a much wider diameter distribution. Despite the morphology of the Cu-doped CZTS nanocrystals also becomes more irregular, they still possess single crystalline structures as revealed by HRTEM studies (Figure 3c,d). The bandgap of the Cu-doped CZTS nanocrystals estimated by UV−vis absorption spectroscopy (Figure 3e) is 1.5 eV, slightly smaller than the undoped CZTS (1.51 eV), which is expected as the EDX composition analysis (not shown) performed on the Cu-doped CZTS nanocrystals gives a formula of $Cu_{2.19}Zn_{0.80}Sn_{0.75}S_{3.53}$ and the excess Cu provides p-type doping.

The electrical and thermal properties of the Cu-doped CZTS nanocrystals are measured on the nanostructured solid disks fabricated through hot press at 523 K for 15 min under an axial pressure of 120 MPa. We decide to use hot press instead of SPS and perform the consolidation process at lower temperature but higher pressure because of the concern of copper diffusion and the SPS safety regulation at Wright-Patterson Air Force Research Lab on handling Cu-rich compounds. Notably, the relative density of the hot pressed Cu-doped CZTS samples is similar to that of spark plasma sintered undoped CZTS samples, which are 89% and 91%, respectively. Figure 4a shows the temperature dependence of Seebeck coefficient of the CZTS nanocrystals with an increasing trend from 65 μV/K at room temperature to 301 μV/K at 700 K. The lower Seebeck coefficient compared to undoped CZTS sample (990 μV/K) is mainly because of the higher carrier concentration from the Cu doping, which, however, is still a 43% increase compared to the Cu-doped CZTS bulk crystals.[25] The electrical conductivity (Figure 4b) of the Cu-doped CZTS nanocrystals increases from 409 S/m at 300 K to 1388 S/m at 700 K, which is about 38 times higher than the undoped CZTS nanocrystal samples (36.7 S/m at 700 K) despite the fact that the relative density of the hot pressed Cu-doped CZTS samples is even still slightly lower than that of spark plasma sintered undoped CZTS samples. The thermal conductivity of the Cu-doped CZTS nanocrystals (black line, Figure 4c) remains low between 300 and 700 K and reaches a minimum of 0.645 W/m·K at 700 K, which corresponds to a 33.5% decrease compared to the undoped CZTS nanocrystal samples (0.97 W/m·K at 700 K). The thermal conductivity reduction in the Cu-doped CZTS nanocrystal samples is mainly because of the lattice distortion when excess Cu dopants occupy the Zn postions in the lattice, which is also consistent with the studies performed on the bulk crystals.[25] Notably, the thermal conductivity observed in our Cu-doped CZTS nanocrystal samples is also 28.3% lower than the Cu-doped CZTS bulk crystals (0.9 W/m·K at 700 K), which can be attributed to the increased phonon scattering at nanocrystal grain boundary observed in the hot pressed disks (inset, Figure 4d). In addition, according to Wiedemann−Franz law, the electron contribution to the total thermal conductivity can be calculated and subtracted to obtain the lattice contribution (red line, Figure 4c), which reaches a minimum of 0.621 W/m·K at 700 K. The overall ZT for the Cu-doped CZTS nanocrystal samples is plotted in Figure 4d, which reaches to the peak value of 0.14 at 700 K, representing a 5.38 times improvement from the undoped CZTS nanocrystal samples.

In summary, we have reported the experimental realization of using nontoxic and abundant CZTS nanocrystals for possible high-temperature thermoelectric energy harvesting. The CZTS nanocrystals can be synthesized in large quantity from solution phase reaction and compressed into robust bulk pellets through SPS and hot press while still maintaining nanoscale grain size inside. Electrical and thermal measurements between 300 and 700 K show significant enhancement in Seebeck coefficient and reduction in thermal conductivity compared to the bulk crystals because of the nanostructuring. Extra copper doping during the nanocrystal synthesis has also dramatically improved the electrical conductivity and reduced the thermal conductivity. The thermoelectric performance of the CZTS nanocrystals could be further improved by optimizing the consolidation process to carefully engineer the grain boundaries and by fine-tuning the copper doping level to improve the power factor, thus making CZTS a competitive alternation not only in performance but also in cost for high temperature (between 600 and 800 K) thermoelectric energy harvesting compared to the conventional tellurides and antimonides.

AUTHOR INFORMATION

Corresponding Author

*E-mail: yuewu@purdue.edu. Telephone: +1-765-494-6028.

ACKNOWLEDGMENTS

Y.W. thanks Purdue University for the new faculty startup grant, Kirk Grant from the Birck Nanotechnology Center, DuPont Young Faculty Award, the Midwest Institute for Nanoelectronics Discovery (MIND), and the NSF/DOE Thermoelectric Partnership (award number 1048616). Y.C. thanks the MIND and the Intel Corporation. Y.W. acknowledges the help from Dr. Douglas Dudis and Charles Cooke at Wright-Patterson Air Force Research Lab on the SPS and the use of the hot press setup at Prof. Chin-Teh Sun's group at Purdue University.

REFERENCES

(1) Kanatzidis, M. G. *Chem. Mater.* **2010**, *22* (3), 648−659.
(2) Vineis, C. J.; Shakouri, A.; Majumdar, A.; Kanatzidis, M. G. *Adv. Mater.* **2010**, *22* (36), 3970−3980.

(3) Lan, Y. C.; Minnich, A. J.; Chen, G.; Ren, Z. F. *Adv. Funct. Mater.* **2010**, *20* (3), 357−376.
(4) DiSalvo, F. J. *Science* **1999**, *285* (5428), 703−706.
(5) Dmitriev, A. V.; Zvyagin, I. P. *Phys.-Usp.* **2010**, *53* (8), 789−803.
(6) Chiritescu, C.; Cahill, D. G.; Nguyen, N.; Johnson, D.; Bodapati, A.; Keblinski, P.; Zschack, P. *Science* **2007**, *315* (5810), 351−353.
(7) Caylor, J. C.; Coonley, K.; Stuart, J.; Colpitts, T.; Venkatasubramanian, R. *Appl. Phys. Lett.* **2005**, *87*, (2).
(8) Venkatasubramanian, R.; Siivola, E.; Colpitts, T.; O'Quinn, B. *Nature* **2001**, *413* (6856), 597−602.
(9) Fan, X. F.; Zeng, G. H.; LaBounty, C.; Bowers, J. E.; Croke, E.; Ahn, C. C.; Huxtable, S.; Majumdar, A.; Shakouri, A. *Appl. Phys. Lett.* **2001**, *78* (11), 1580−1582.
(10) Koga, T.; Sun, X.; Cronin, S. B.; Dresselhaus, M. S. *Appl. Phys. Lett.* **1998**, *73* (20), 2950−2952.
(11) Androulakis, J.; Lin, C. H.; Kong, H. J.; Uher, C.; Wu, C. I.; Hogan, T.; Cook, B. A.; Caillat, T.; Paraskevopoulos, K. M.; Kanatzidis, M. G. *J. Am. Chem. Soc.* **2007**, *129* (31), 9780−9788.
(12) Wang, H.; Li, J. F.; Nan, C. W.; Zhou, M.; Liu, W. S.; Zhang, B. P.; Kita, T. *Appl. Phys. Lett.* **2006**, *88*, (9).
(13) Sootsman, J. R.; Pcionek, R. J.; Kong, H. J.; Uher, C.; Kanatzidis, M. G. *Chem. Mater.* **2006**, *18* (21), 4993−4995.
(14) Poudeu, P. F. P.; D'Angelo, J.; Downey, A. D.; Short, J. L.; Hogan, T. P.; Kanatzidis, M. G. *Angew. Chem., Int. Ed.* **2006**, *45* (23), 3835−3839.
(15) Hsu, K. F.; Loo, S.; Guo, F.; Chen, W.; Dyck, J. S.; Uher, C.; Hogan, T.; Polychroniadis, E. K.; Kanatzidis, M. G. *Science* **2004**, *303* (5659), 818−821.
(16) Harman, T. C.; Taylor, P. J.; Walsh, M. P.; LaForge, B. E. *Science* **2002**, *297* (5590), 2229−2232.
(17) Poudel, B.; Hao, Q.; Ma, Y.; Lan, Y.; Minnich, A.; Yu, B.; Yan, X.; Wang, D.; Muto, A.; Vashaee, D.; Chen, X.; Liu, J.; Dresselhaus, M. S.; Chen, G.; Ren, Z. *Science* **2008**, *320* (5876), 634−638.
(18) Joshi, G.; Lee, H.; Lan, Y. C.; Wang, X. W.; Zhu, G. H.; Wang, D. Z.; Gould, R. W.; Cuff, D. C.; Tang, M. Y.; Dresselhaus, M. S.; Chen, G.; Ren, Z. F. *Nano Lett.* **2008**, *8* (12), 4670−4674.
(19) Wang, X. W.; Lee, H.; Lan, Y. C.; Zhu, G. H.; Joshi, G.; Wang, D. Z.; Yang, J.; Muto, A. J.; Tang, M. Y.; Klatsky, J.; Song, S.; Dresselhaus, M. S.; Chen, G.; Ren, Z. F. *Appl. Phys. Lett.* **2008**, *93*, 19.
(20) *Mineral Commodity Summaries 2011*; U.S. Department of the Interior, U.S. Geological Survey: Reston, VA, 2011; http://minerals.usgs.gov/minerals/pubs/mcs/2011/mcs2011.pdf .
(21) *Hazardous Substances Data Bank*; U.S. National Library of Medicine: Bethesda, MD; http://toxnet.nlm.nih.gov/cgi-bin/sis/htmlgen?HSDB.
(22) Steinhagen, C.; Panthani, M. G.; Akhavan, V.; Goodfellow, B.; Koo, B.; Korgel, B. A. *J. Am. Chem. Soc.* **2009**, *131* (35), 12554−12555.
(23) Gibson, J. M.; Lanzerotti, M. Y.; Elser, V. *Appl. Phys. Lett.* **1989**, *55* (14), 1394−1396.
(24) Lauhon, L. J.; Gudiksen, M. S.; Wang, D.; Lieber, C. M. *Nature* **2002**, *420* (6911), 57−61.
(25) Liu, M.-L.; Huang, F.-Q.; Chen, L.-D.; Chen, I.-W. *Appl. Phys. Lett.* **2009**, *94* (20), 202103.
(26) Kumar, Y. B. K.; Babu, G. S.; Bhaskar, P. U.; Raja, V. S. *Phys. Status Solidi A* **2009**, *206* (7), 1525−1530.
(27) Smith, A. M.; Nie, S. *Acc. Chem. Res.* **2009**, *43* (2), 190−200.
(28) Guo, Q.; Hillhouse, H. W.; Agrawal, R. *J. Am. Chem. Soc.* **2009**, *131* (33), 11672−11673.
(29) Riha, S. C.; Parkinson, B. A.; Prieto, A. L. *J. Am. Chem. Soc.* **2009**, *131* (34), 12054−12055.
(30) Jenkins, R.; Gould, R. W.; Gedcke, D. *Quantitative x-ray spectrometry*; CRC Press: New York, 1995.
(31) Hicks, L. D.; Harman, T. C.; Dresselhaus, M. S. *Appl. Phys. Lett.* **1993**, *63* (23), 3230−3232.
(32) Hicks, L. D.; Dresselhaus, M. S. *Phys. Rev. B* **1993**, *47* (19), 12727−12731.
(33) Vashaee, D.; Shakouri, A. *Phys. Rev. Lett.* **2004**, *92*, 10.
(34) Norris, D. J.; Efros, A. L.; Erwin, S. C. *Science* **2008**, *319* (5871), 1776−1779.
(35) Erwin, S. C.; Zu, L. J.; Haftel, M. I.; Efros, A. L.; Kennedy, T. A.; Norris, D. J. *Nature* **2005**, *436* (7047), 91−94.